Journal of
Composites Science

MDPI

Article

Experimental Study on Permeability and Infusion Simulation of Automatically Placed Dry Fiber Preforms

Wei Du [1,2], Jun Liu [1], Hao Song [1,2], Minqiang Jiang [1,2,*], Bo Ning [3], Yang Yang [3], Weiping Liu [3], Keqing Han [1,*], Hui Zhang [1,2] and Jianyong Yu [2]

[1] State Key Laboratory of Advanced Fiber Materials, College of Materials Science and Engineering, Donghua University, Shanghai 201620, China
[2] Center for Civil Aviation Composites, College of Materials Science and Engineering, Donghua University, Shanghai 201620, China
[3] Composite Materials Center, Shanghai Aircraft Manufacturing Co., Ltd., Shanghai 201324, China
* Correspondence: minqiang.jiang@outlook.com (M.J.); hankeqing@dhu.edu.cn (K.H.)

Abstract

To investigate the resin infusion molding process for novel dry fiber-reinforced epoxy composite wing skin, dry fiber preforms were fabricated via an automated fiber placement (AFP) system, and the out-of-plane permeability of the preforms at different lay-up speeds was measured using the ultrasonic transmission method to determine the optimal lay-up parameters. A scaled-down composite wing skin structure was modeled and meshed via numerical simulation, and different resin infusion schemes were simulated and analyzed using PAM-RTM software. The optimal infusion scheme was determined by comparing the infusion time, infusion pressure and defect formation during resin flow for different schemes, and the wing skin component was fabricated through the vacuum-assisted resin infusion (VARI) process. Results indicate that the infusion time predicted by PAM-RTM simulation is 3883 s, while the actual measured value in the VARI process is 3611 s with an error of approximately 7% within a reasonable range. Both simulation and actual wing skin fabrication exhibited no significant defects, validating the accuracy of the three-dimensional permeability measurement of dry fiber preforms as well as the reliability of the simulation results.

Keywords: dry fiber composite materials; vacuum-assisted resin infusion molding; PAM-RTM; resin flow simulation

Academic Editors: Jiadeng Zhu and Hyunjin Cho

Received: 17 March 2026
Revised: 3 May 2026
Accepted: 12 May 2026
Published: 21 May 2026

1. Introduction

Carbon fiber-reinforced composites are widely used in aerospace, rail transportation automotive, marine, wind power and other fields due to their advantages of being lightweight, having high strength, and exhibiting corrosion resistance. These materials have become essential for achieving lightweighting in products [1–3]. In recent years, dry fiber automated placement-liquid molding technology has achieved remarkable development as a representative low-cost composite manufacturing method [4]. This process starts with the preparation of dry fiber preforms via automated placement technology. Subsequently, composite components are fabricated using liquid composite molding (LCM) techniques, including resin transfer molding (RTM) and vacuum-assisted resin infusion (VARI) [5]. Dry fiber liquid molding exhibits numerous distinct advantages. It reduces manufacturing costs, increases production efficiency, and delivers superior dimensional accuracy. This method also ensures high structural integrity and consistent quality throughout the manufacturing

process, making it especially well-suited for the efficient production of large, complex components [6,7].

In liquid composite molding (LCM) processes, the placement of fiber preforms within the mold, resin injection, and the curing stage all significantly impact the final product quality [8,9]. Particularly during resin filling, issues such as uneven resin flow, insufficient fiber impregnation, and localized resin deficiency or excess within the preform may arise [10,11]. The design of the resin injection affects the overall flow path and filling time of the resin, thereby influencing the permeability uniformity of the resin in the fiber preform and the stability of the flow front [12,13]. This challenge becomes significantly pronounced when manufacturing large-scale, complex, and irregularly shaped components, where geometric complexity and material anisotropy not only easily lead to undesirable resin flow behavior, air entrapment, and incomplete impregnation, but also make the identification of optimal injection gate and vent placements extremely difficult [14]. Traditionally, manual trial-and-error methods have been employed for prototyping, leading to low efficiency and high production costs. Therefore, the analysis of resin flow behavior based on numerical simulation can provide key parameters such as resin pressure distribution and the evolution of the flow front. This enables an intuitive visualization of the entire resin infusion process and offers actionable guidance for industrial production and processing [15,16].

The coupled finite element/control volume technique adopts the finite element method to solve the governing equations of the pressure field and utilizes the control volume scheme to track the position of the resin flow front, making it highly suitable for the numerical simulation of resin infusion and mold filling [17]. Meanwhile, this technique also constitutes the fundamental algorithmic basis of the PAM-RTM software. Laurenzi et al. [18] analyzed the effects of injection gate location, injection pressure, and mold design on resin flow in the liquid molding process via finite element simulation analysis. Results demonstrated that finite element simulation effectively reduced defect formation and improved production efficiency. Rodrigues et al. [19] employed PAM-RTM software to investigate the effect of different injection pressures on resin impregnation of fiber preforms. Results demonstrated good agreement between numerical simulations and experimental data for resin flow front, filling time, and filling pressure. Koziol et al. [20] simulated the VARI process using PAM-RTM software. Results indicated that experimental and simulated errors for resin front and process time ranged from a few percent to over ten percent. Grössing et al. [21] demonstrated that PAM-RTM software can predict the temporal evolution of the flow front during resin infusion and defects such as dry spots within structural components. Khalili et al. [22] conducted resin infusion experiments and simulations for fiber-reinforced composites. Results showed high consistency between the experimental flow front and simulation predictions.

Accurate permeability values are essential for achieving a more precise simulation of the resin infusion process. Magagnato et al. [23] measured the in-plane permeability of fabrics, manufactured components with insert-containing fiber preforms using liquid composite molding, and performed numerical simulation and experimental validation of the resin infusion process with PAM-RTM. The results showed that the inserts caused local deformation of the fibers. Kim et al. [24] measured the in-plane permeability of fabrics with deformed fiber orientations, and then simulated the liquid molding process of a U-shaped composite structure using PAM-RTM software, finding that the simulated resin flow front and filling time matched experimental results. Falaschetti et al. [25] measured the permeability of reinforced fabrics experimentally and simulated the resin infusion process of components in the RTM process using PAM-RTM software. The results showed that the discrepancy between experimental and simulated values was small, and no dry spots, voids or other defects were found on the surface of the parts after demolding. Siddig et al. [26] nu-

merically predicted material permeability from 3D fabric scanning data. The permeability tensor, as a key input, was imported into PAM-RTM for process simulation. Results show that the model enables multi-scenario numerical prediction and supports monitoring and decision-making during composite component resin infusion. Chen et al. [27] measured the three-dimensional permeability of carbon fiber reinforcements for manufacturing automotive floor panels, and performed three-dimensional filling simulations using PAM-RTM software. The results demonstrated that peripheral injection significantly improved the resin infusion efficiency.

This study adopts novel dry fiber materials and prepares dry fiber preforms by an automated placement process. The through-thickness permeability of the preforms at different lay-up speeds is measured using the ultrasonic transmission method, and the optimal lay-up process parameters are determined. On this basis, a numerical model of the dry fiber composite wing skin is established, and comparative simulations of different resin infusion schemes in the VARI process are conducted using PAM-RTM software to identify the optimal scheme. Finally, the feasibility and prediction accuracy of the numerical simulation method are verified by molding experiments.

2. Materials and Methods

2.1. Materials

The reinforcement tape used in this study to fabricate preforms was a newly developed T800 fabric (200 g/m^2) compatible with automated fiber placement (AFP) equipment, supplied by Changzhou Xinchuang Intelligent Technology Co., Ltd., Changzhou, China, which consists of two other materials called binder and veil in addition to fibers.The schematic diagram of the structure of the dry fiber material is shown in Figure 1.

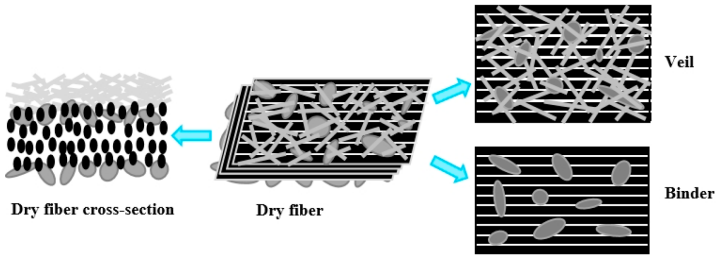

Figure 1. Schematic diagram of the structure of dry fiber material.

The epoxy resin used for the composites was 3325 (viscosity 0.837 Pa s at 20 °C) provided by Guangdong Yutongda Advanced Materials Co., Ltd., Guangzhou, China. Peel ply (PU85) and vacuum bag film (VBF204) were obtained from Granudan Surface Technology (Shanghai) Co., Ltd., Shanghai, China. Tape (butyl rubber) and spiral tube (polyethylene) and vacuum tube (polytetrafluoroethylene) were produced by Hongju Composite Materials Co., Ltd., Handan, China. T-shaped tee joint (outer diameter: 8 mm) and ball valve (outer diameter: 8 mm) were supplied by Zhejiang Qiai Co., Ltd., Zhuji, China. Mold release agent (PMR-EZ) was obtained from Chem-Trend (Shanghai) Trading Co., Ltd., Shanghai, China.

2.2. Main Instruments and Equipment

Automatic Fiber Placement (AFP) equipment (Cross–layer, M & A Dieterle GmbH, Ottenbach, Germany), vacuum pump (V-i120SV, Zhejiang Feiyue Electromechanical Co., Ltd., Jinhua, China), and Thermostatic drying oven (YB-1, Shanghai Yibo Industry Co., Ltd., Shanghai, China).

2.3. Theoretical Model for Radial and Out-of-Plane Permeability

The permeability of carbon fiber fabrics was assessed via unsaturated linear flow tests. Herein, during the liquid molding infusion process, the flow of resin through carbon fiber fabrics can be deemed as fluid flow in porous media, and such flow behavior within porous media is governed by Darcy's law [28]:

$$\nu = -\frac{1}{\mu} K \nabla P \tag{1}$$

ν is the superficial velocity of the fluid; K is the permeability tensor; μ is the viscosity of the fluid; ∇P is the pressure gradient.

Two-dimensional permeability is also referred to as radial permeability. In two-dimensional permeability measurements, fluid is injected into the carbon fiber fabric at a specific out-of-plane position. Depending on the fabric architecture, the permeability values may differ along different directions. The present experimental study mainly characterizes the resin flow behavior in the two in-plane directions, whose governing theoretical expression is the two-dimensional Darcy's law:

$$\begin{bmatrix} \frac{u_x}{u_y} \end{bmatrix} = -\frac{1}{\mu} \begin{bmatrix} K_{xx} & K_{xy} \\ K_{yx} & K_{yy} \end{bmatrix} \begin{bmatrix} \frac{\partial P}{\partial x} \\ \frac{\partial P}{\partial y} \end{bmatrix} \tag{2}$$

u_x and u_y denote the resin filling velocities in the x and y directions; K_{xx}, K_{xy}, K_{yx}, and K_{yy} are the components of the two-dimensional permeability tensor; $\frac{\partial P}{\partial x}$ and $\frac{\partial P}{\partial y}$ stand for the pressure gradients in the x and y directions.

Combined with the continuity equation for incompressible fluid flow:

$$\frac{\partial u_x}{\partial x} + \frac{\partial u_y}{\partial y} = 0 \tag{3}$$

Furthermore, as the PAM-RTM 2021 software allows for the definition of permeability directions, the permeability along the main and auxiliary permeability directions can be directly measured during the characterization of carbon fiber fabric permeability, without requiring alignment between these main/auxiliary directions and the fabric's warp and weft orientations. Owing to the orthotropic nature of permeability along the main and auxiliary directions, the mold filling front of the reinforced fabric will adopt an approximately elliptical shape, and the permeability tensor can thus be expressed as:

$$K = \begin{bmatrix} K_{xx} & 0 \\ 0 & K_{yy} \end{bmatrix} \tag{4}$$

Through polar coordinate transformation, combined with the condition of constant-pressure injection and the relationship between the actual fluid flow velocity in the pores of the porous medium and the average flow velocity, the relationship between the resin filling front position and time is obtained via integration. The permeability value can then be derived through rearrangement [29]:

$$K_{xx} = \frac{\mu\varepsilon}{4t\Delta P}\left\{r_x^2\left[2\ln\left(\frac{r_x}{r_0}\right) - 1\right] + r_0^2\right\} \tag{5}$$

$$K_{yy} = \frac{\mu\varepsilon}{4t\Delta P}\left\{r_y^2\left[2\ln\left(\frac{r_y}{r_0}\right) - 1\right] + r_0^2\right\} \tag{6}$$

r_x and r_y are the radii of the fluid flow front in the main and auxiliary permeability directions; r_0 is the radius of the resin injection gate; ε is the porosity of the preform.

In this work, the dry fiber preforms were fabricated by AFP through layer-by-layer placement under heating and compaction, which is expected to provide relatively stable preform architecture and reduce the influence of thickness variation to some extent. In addition, the main purpose of this study is to comparatively evaluate the permeability behavior of preforms prepared at different AFP speeds, rather than to establish an exact permeability model for a fully coupled compaction–flow process. It should be noted that Equations (5) and (6) are typically derived for resin transfer molding (RTM) with rigid molds, where the preform thickness is assumed to remain constant during infusion. Therefore, although the vacuum-assisted resin infusion (VARI) process involves flexible tooling, the constant-thickness assumption may still be regarded as an acceptable engineering approximation for the comparative permeability evaluation in this study using Equations (5) and (6), with its applicability limited to the present conditions.

As in the treatment of permeability under two-dimensional conditions, the method of transforming the anisotropic actual flow plane into an isotropic equivalent system is also adopted in the out-of-plane permeability measurement. The permeability is mainly calculated based on the flow front positions measured at different times, and the out-of-plane permeability can thus be expressed as follows [30]:

$$K_{zz} = \frac{\mu\varepsilon {r_0}^2}{6t\Delta P}\left\{2\left(\frac{r_z}{r_0}\right)^3 - 3\left(\frac{r_z}{r_0}\right)^2 + 1\right\} \quad (7)$$

r_z is the radius of the fluid flow front in the out-of-plane permeability direction.

2.4. Preparation of Dry Fiber Preforms

2.4.1. Preparation of Dry Fiber Preforms for Three-Dimensional Permeability Measurement

In this study, dry fiber preforms (230 mm × 250 mm) were fabricated via a cross-layer automated fiber placement (AFP) system (Figure 2). Geometric modeling and tow path planning were first conducted using CAD 2022 software to generate the dedicated AFP control program. Preforms for in-plane permeability testing with 4 layers were manufactured at a layup pressure of 4 bar and a fiber placement speed of 200 mm/s. For out-of-plane permeability characterization, 10-layer preforms were prepared at a constant 4 bar pressure with three placement speeds: 250 mm/s corresponding to an unmelted veil, 200 mm/s to a partially melted veil, and 150 mm/s to a fully melted veil. A 1 mm gap between adjacent tows and a 3.175 mm interlayer offset were applied to avoid tow overlapping. The forming quality was monitored and regulated in real time during the placement process, and the finished preforms were demolded afterward.

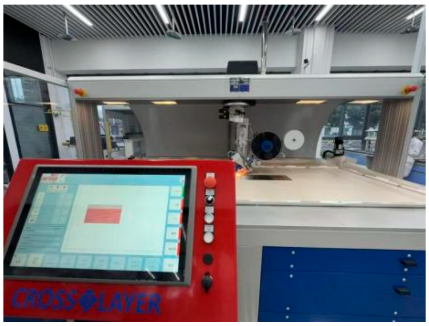

Figure 2. Automatic fiber placement (AFP) equipment.

2.4.2. Preparation of Dry Fiber Preforms for Wing Skin

In this study, dry fiber preforms were laid up using an automatic fiber placement machine, and then fiber-reinforced composites were fabricated via the vacuum assisted

resin infusion (VARI) process. Considering the feasibility of matching dry fiber materials and the automatic fiber placement equipment, a scaled-down prototype of a typical wing skin structural component with a certain curvature was selected for the research. The typical structural component is illustrated in Figure 3, and its projected dimensions are 300 mm × 200 mm × 1.7 mm. The wing skin structural component is mainly composed of two circular arcs with different radii, with an overall projected length of 200 mm. The longer curved surface has a radius of 3000 mm and a projected length of 245 mm; the shorter curved surface has a radius of 300 mm and a projected length of 55 mm. The dry fiber tows were laid up in accordance with the stacking sequence of $[45/-45/0/0/90]_s$, with a total of 10 layers in the thickness direction. The dry fiber tows were grouped into bundles of four, with a 1 mm gap introduced between adjacent fiber tapes during the lay-up process.

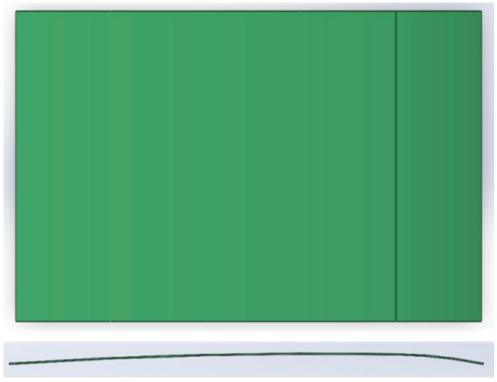

Figure 3. Solid model of wing skin: front view (**top**); left view (**bottom**).

2.5. Determination of Three-Dimensional Permeability of Dry Fiber Preforms

2.5.1. Determination of In-Plane Permeability of Dry Fiber Preforms

In this study, the unsaturated radial flow method was adopted to determine the in-plane permeability of dry fiber preforms. The permeability testing device for dry fiber preforms used in this study is illustrated in Figure 4. The dry fiber preforms were cut to the required size, and then placed sequentially on a clean glass plate mold, followed by the release fabric and vacuum bag film. A sealed system was constructed around the dry fiber preform using sealing tape, three-way valves, and infusion tubes. A vacuum pump was used to draw a vacuum; once the reading of the vacuum pump stabilized, the camera of the in-plane permeability test device for dry fiber preforms and the valve of the resin injection gate at the center of the dry fiber preform were opened simultaneously. The ambient temperature was maintained at a constant value of 20 °C.

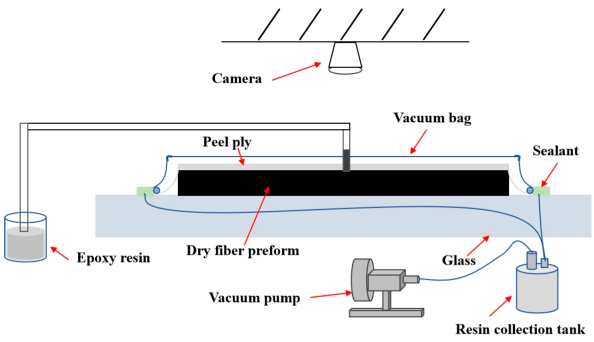

Figure 4. Permeability testing device for dry fiber preforms.

2.5.2. Determination of Out-of-Plane Permeability of Dry Fiber Preforms

The ultrasonic transmission technique was adopted to measure the permeability of dry fiber preforms in the thickness direction. An ADIPR automatic ultrasonic testing system (Donghua University, Shanghai, China.) equipped with 1 MHz contact probes was used. Figure 5 schematically illustrates the principle for determining the position of the resin flow front in the thickness direction. As shown in the diagram, the preform is positioned between the upper and lower molds. The resin is introduced into the mold cavity through the central inlet of the lower mold and then gradually impregnates the preform. Since the propagation velocity of ultrasonic waves differs between dry fibers and infiltrated fibers, as the resin continuously flows into the preform, the time required for ultrasonic waves to transmit through the preform (i.e., Time of Flight (TOF)) decreases gradually. The difference in this time variation can be used to measure the position of the resin flow front in the thickness direction in real time, and then the permeability in the thickness direction can be calculated accordingly.

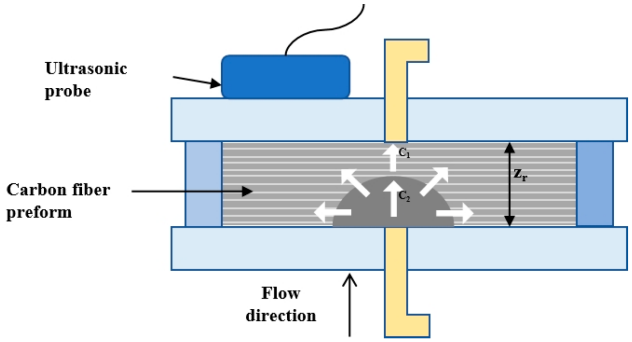

Figure 5. Principle of flow front measurement via ultrasonic transmission method.

3. Results

3.1. Results of Three-Dimensional Permeability Determination for Dry Fiber Preforms

3.1.1. Results of In-Plane Permeability Determination

The in-plane permeability measurement setup is shown in Figure 6. The position of the resin flow front during the determination of the dry fiber preform was recorded by the camera. The position of the 3325-epoxy resin flow front at time t in the principal and secondary permeability directions was recorded. The resin flow front in the x-direction was denoted as r_x and that in the y-direction as r_y.

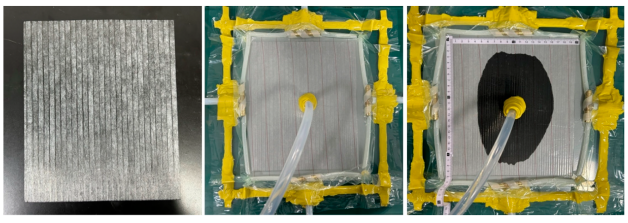

Figure 6. In-plane permeability measurement of dry fiber preform.

The linear fitting results of resin filling front position and perfusion time t are shown in Figure 7. The main permeability of the dry fiber preform is $K_{xx} = 1.8 \times 10^{-11}$ m^2, and the auxiliary permeability is $K_{yy} = 9.8 \times 10^{-12}$ m^2. Due to the diversion effect of the in-plane gap and the fiber, the permeability of the dry fiber preform in the fiber direction is higher than that perpendicular to the fiber direction.

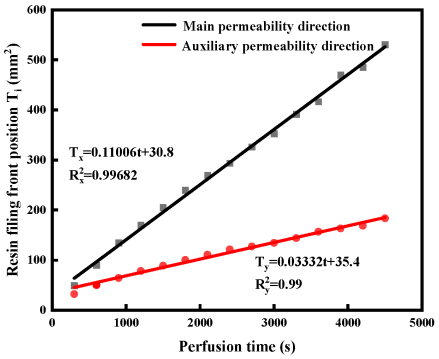

Figure 7. Fitting results of resin filling front position in the main/auxiliary permeability direction of dry fiber performs.

3.1.2. Results of Out-of-Plane Permeability Determination

In the out-of-plane permeability measurement, the ADIPR automatic ultrasonic testing system equipped with 1 MHz contact probes was adopted. This setup reliably identifies the fluid front in dry fiber preforms with minimal signal attenuation. The dry fiber preforms fabricated at AFP speeds of 250 mm/s, 200 mm/s, and 150 mm/s are shown in Figure 8. The measured total infiltration times for these preforms were 2800 s, 2900 s, and 6200 s, respectively. The corresponding flow front position–time curves are presented in Figure 9, and the calculated out-of-plane permeability–time curves are shown in Figure 10. The final out-of-plane permeability values (K_{zz}) are presented in Figure 11.

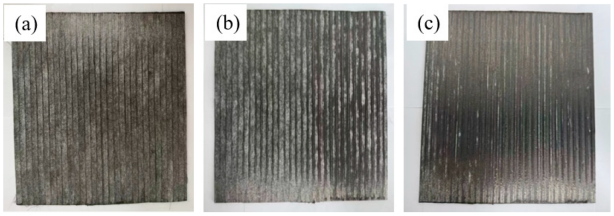

Figure 8. Dry fiber preforms: (**a**) 250 mm/s, (**b**) 200 mm/s, (**c**) 150 mm/s.

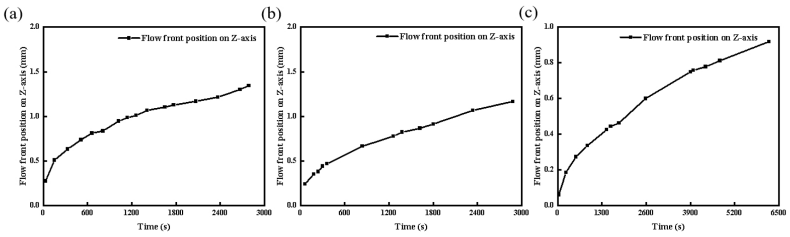

Figure 9. Flow front position–time curves of dry fiber preforms: (**a**) 250 mm/s, (**b**) 200 mm/s, (**c**) 150 mm/s.

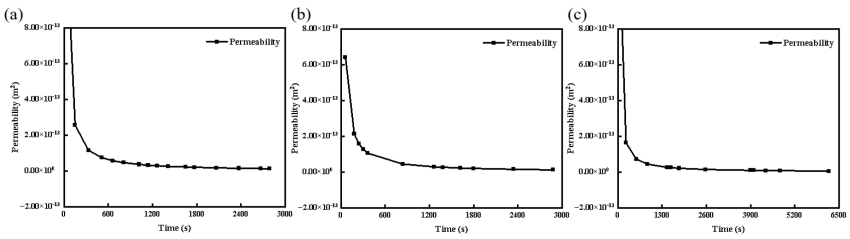

Figure 10. Out-of-plane permeability–time curves of dry fiber preforms: (**a**) 250 mm/s, (**b**) 200 mm/s, (**c**) 150 mm/s.

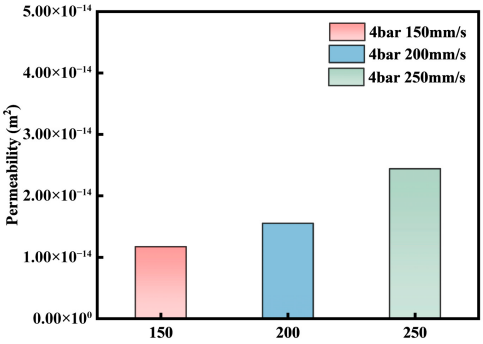

Figure 11. Out-of-plane permeability data of dry fiber preforms.

The results show a clear inverse relationship between AFP speed and out-of-plane permeability. K_{zz} decreases from 2.44 × 10^{-14} m^2 at 250 mm/s to 1.55 × 10^{-14} m^2 at 200 mm/s, and further to 1.17 × 10^{-14} m^2 at 150 mm/s. At a high placement speed of 250 mm/s, the short dwell time under the heating roller results in insufficient heat transfer, leading to only partial melting of the veil. Interlayer bonding remains weak and fails to satisfy the manufacturing requirements for lay-up, forming and fabrication of typical structural components. In contrast, at 150 mm/s, the complete melting of the veil results in excellent interlayer fixation, but it also drastically reduces the through-thickness permeability. The resin mold-filling and impregnation along the thickness direction is significantly hindered with low penetration efficiency, which is also unsuitable for the forming and manufacturing of typical structural components, making resin impregnation highly inefficient as reflected by the longest infiltration time of 6200 s. At the intermediate speed of 200 mm/s, a balanced state is achieved in which the veil partially melts, providing sufficient interlayer bonding. This yields a moderate permeability of 1.55 × 10^{-14} m^2 and a reasonable infiltration time of 2900 s, representing the optimal process window for manufacturing wing skin components. Therefore, despite the good interlayer fixation at 150 mm/s, the excessively low permeability makes it unsuitable for thick or large-scale structural parts.

3.2. Numerical Simulation of Resin Infusion Process for Liquid Molding of Wing Skin

3.2.1. Establishment of Wing Skin Model

The solid model of wing skin is established by using three-dimensional modeling software SolidWorks2024. The 3D model of the wing skin, including dry fiber tows and gaps, is shown in Figure 12. In order to accurately simulate the flow path of resin between dry fiber layers, not only the modeling of dry fiber tows should be considered, but also the gap modeling between dry fiber tows should be considered. In this paper, a 3D model was established for each layer of dry fiber tows and gaps. Due to the variable curvature structure of the wing skin, the matching problem between layers should also be considered in the modeling.

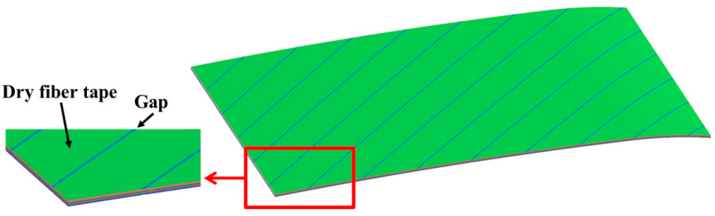

Figure 12. 3D model of wing skin.

The built model is imported into HyperMesh 2021 software for triangular mesh generation. The triangular mesh possesses favorable adaptability, allowing it to better fit the curvature variation of the wing skin. The number of finite element mesh elements of the model is 670,523, and the number of nodes is 174,826. The model after meshing is shown in Figure 13.

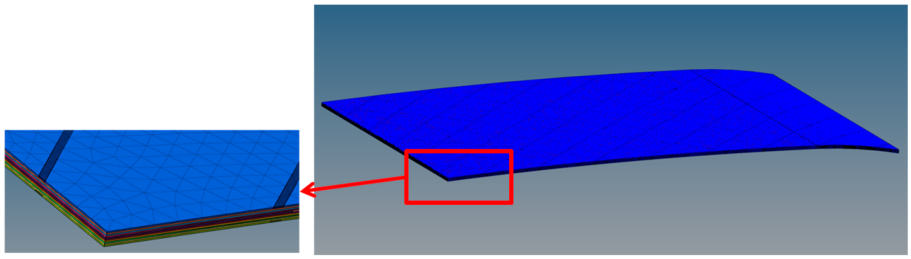

Figure 13. Mesh generation of wing skin model.

3.2.2. Material Properties

Material parameters including resin density, resin viscosity, injection pressure, fiber volume fraction, and three-dimensional permeability of dry fiber preforms were assigned to the wing skin model. The resin flow analysis of the wing skin model in this study was carried out under the process conditions of VARI, and the specific parameters are listed in Table 1.

Table 1. Basic material and process parameters.

Parameter	Numerical Value
Resin Density/(g/cm^3)	1.15
Resin Viscosity/(Pa·s)	0.83
Injection Pressure/MPa	0.099
Fiber Volume Fraction/%	64
Fiber Permeability in X-direction (K_{xx}/m^2)	1.8×10^{-11}
Fiber Permeability in Y-direction (K_{yy}/m^2)	9.8×10^{-12}
Fiber Permeability in Z-direction (K_{zz}/m^2)	1.55×10^{-14}

3.2.3. Design of Resin Injection Scheme

The injection design must be closely integrated with the structural characteristics of the wing skin, which exhibits significant variations in surface curvature and consists of large-area thin-walled curved structures. Considering the structural symmetry, the four injection schemes were designed, as illustrated in Figure 14. In the figure, the yellow elements represent the resin injection gates, and the red elements represent the resin outlet vents.

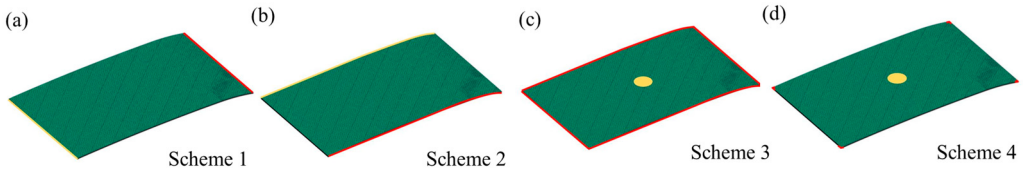

Figure 14. Resin injection schemes for wing skin: (**a**) Scheme 1, (**b**) Scheme 2, (**c**) Scheme 3, (**d**) Scheme 4.

In Scheme 1, a continuous linear injection gate (yellow) is placed at the root of the short edge with a larger radius (R = 3000 mm), while a continuous linear vent (red) is placed along the opposite short edge with a smaller curvature radius (R = 300 mm). In Scheme 2, a continuous linear injection gate runs along the long edge (yellow), and a continuous linear

vent is placed along the symmetrically opposite long edge (red). Scheme 3 replaces linear injection with point injection. A single 9 mm diameter injection gate (yellow) is placed at the center of the wing skin, and continuous linear vents are arranged around the perimeter (red). Scheme 4 replaces linear vents with point vents. A single 9 mm injection gate (yellow) remains at the center, while discrete point vents are placed at the four corners (red). In all four schemes, a flow medium is applied to the upper surface of the wing skin.

3.2.4. Analysis of Simulation Results for Wing Skin

After setting the relevant simulation parameters and the positions of resin injection gates and vents, numerical calculations were performed using PAM-RTM software. The distributions of filling degree, filling time, and filling pressure for the wing skin are presented in Figures 15–17.

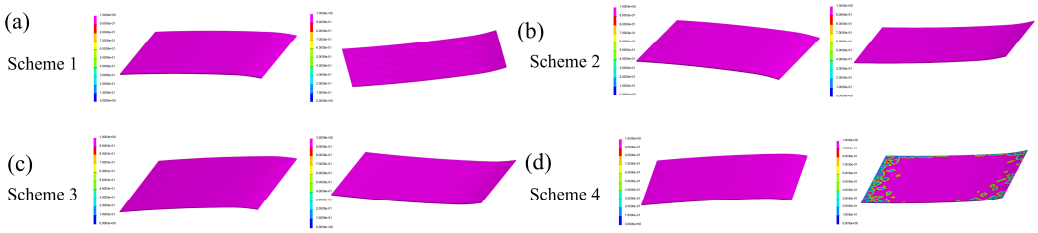

Figure 15. Filling degree contour plots: (**a**) Scheme 1, (**b**) Scheme 2, (**c**) Scheme 3, (**d**) Scheme 4.

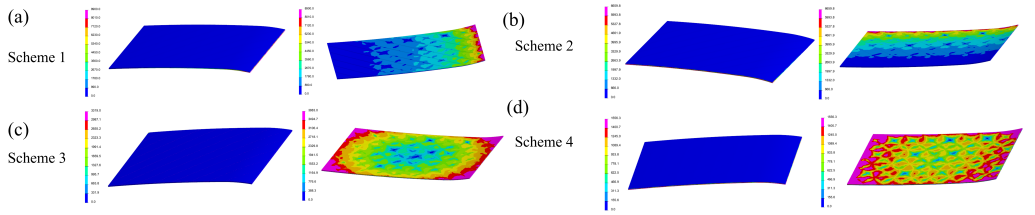

Figure 16. Filling time contour plots: (**a**) Scheme 1, (**b**) Scheme 2, (**c**) Scheme 3, (**d**) Scheme 4.

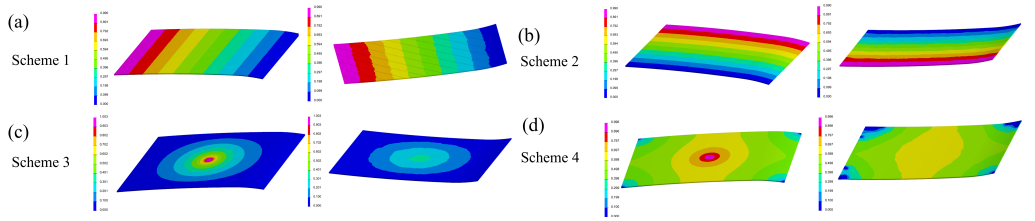

Figure 17. Filling pressure contour plots: (**a**) Scheme 1, (**b**) Scheme 2, (**c**) Scheme 3, (**d**) Scheme 4.

Figure 15 shows the filling degree contour plots for the four injection schemes. In these plots, the color gradient from blue to red represents the filling state from unfilled to fully filled. Schemes 1, 2, and 3 achieve complete resin filling over the entire wing skin, including highly curved regions, with no dry spots or voids. This indicates that continuous linear gates (Schemes 1 and 2) as well as a point gate with perimeter vents (Scheme 3) provide effective flow coverage and air evacuation. In contrast, Scheme 4 fails to fully impregnate the component. Dry spots appear at the corners and on high-curvature surfaces, suggesting that discrete point vents at the four corners are insufficient to guide resin into these geometrically complex areas. Thus, Scheme 4 is unsuitable for the wing skin geometry.

An in-depth analysis was conducted on the simulation results. Figure 16 presents the filling time contour plots for the four injection schemes. In Scheme 1, the total filling time is approximately 8900 s. The flow medium enables rapid surface infiltration, effectively converting the linear injection into a surface infusion mode. However, due to the variable

curvature of the wing skin, the right corner region with high curvature (red area) exhibits a significantly longer filling time. This delay increases the risk of resin gelation before complete impregnation, which can lead to dry spots and voids in practice.

Scheme 2 shows a shorter filling time of 6659 s. The contour plot displays a large blue-green region and a small red region, indicating relatively uniform resin penetration and reduced impregnation time. Scheme 3 further reduces the filling time to 3883 s, with the peripheral regions being the last to saturate. Scheme 4 gives the shortest filling time of 1556 s. However, as shown in Figure 16d, the resin flow front velocity attenuates rapidly with increasing diffusion distance. This results in a large discrepancy in impregnation time between interlaminar gaps and the dry fiber preform, leading to non-uniform resin penetration and a high likelihood of dry spot formation. Thus, Scheme 4 is not recommended for the wing skin geometry.

Figure 17 shows the filling pressure contour plots for the four injection schemes. The pressure distribution provides an indirect indication of the resin flow front behavior. In Scheme 1, the low-pressure region occupies a large proportion, indicating that the resin experiences little flow resistance over most of the wing skin. However, this also suggests a relatively slow impregnation rate within the dry fiber preform, as a lower pressure gradient reduces the driving force for resin flow. In Scheme 2, the pressure decreases gradually from the injection gate toward the vent along the flow front, reflecting a stable and progressive filling pattern. Scheme 3 exhibits a similar gradual pressure decrease, with continuous, uniform, and gentle pressure variations. This indicates a well-balanced injection configuration that maintains a steady flow front without abrupt pressure jumps, making it a reasonable design for the wing skin geometry. In Scheme 4, the pressure also decreases gradually from the gate to the vents. However, localized pressure jump regions appear at the four corner vents, accompanied by two "blue spots" on the left side of the wing skin. These pressure jumps disrupt the uniformity of resin impregnation, leading to non-uniform flow and a high likelihood of dry spot formation. Therefore, Scheme 4 is not recommended.

Table 2 summarizes the simulation results for the four infusion schemes. The use of an in-plane flow medium effectively converts the resin injection mode from linear flow to a more uniform planar infusion, thereby improving impregnation uniformity within the dry fiber preform. Schemes 3 and 4 show significant advantages in infusion time. However, in Scheme 4, the resin travel distance to the four corners is relatively long, which increases the risk of dry spots and voids due to delayed filling and potential air entrapment. In contrast, Scheme 3 exhibits more uniform resin flow toward the edges and gentler filling pressure variations, leading to a lower probability of defect formation. Consequently, Scheme 3 is selected as the optimal mold-filling scheme for the wing skin.

Table 2. Simulation results of resin injection schemes for wing skin.

Resin Injection Scheme	Filling Time/s	Presence of Dry Spots
Resin injection scheme 1	8900	No
Resin injection scheme 2	6659	No
Resin injection scheme 3	3883	No
Resin injection scheme 4	1556	Yes

3.3. Molding and Analysis of Wing Skin

3.3.1. Process Flow of Vacuum-Assisted Resin Infusion (VARI) for Wing Skin Molding

The main process for fabricating dry fiber wing skin components using the VARI process is illustrated in Figure 18. An appropriate amount of release agent is evenly applied

to the mold surface with clean gauze. Subsequently, the dry fiber preform is placed onto the mold surface. Construct a sealed boundary along the mold platform using sealant. Sequentially lay down the peel ply, flow medium, and vacuum bag. Resin injection gates and vents are established using three-way valves, flow guide tubes, and polytetrafluoroethylene (PTFE) tubing. The assembly is then inspected for airtightness. Excellent sealing performance with no leakage points is confirmed, satisfying the requirements for the subsequent resin infusion process.

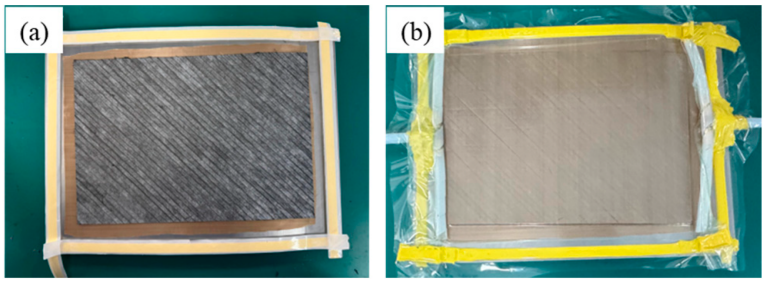

Figure 18. VARI forming process: (**a**) Laying peel ply, (**b**) vacuum bag sealing.

3.3.2. Experimental Analysis of Vacuum-Assisted Resin Infusion (VARI) for Wing Skin

During the VARI process of the wing skin, resin is infused into the dry fiber preform inside the flexible vacuum bag by the pressure difference between atmospheric pressure and vacuum pressure. The filling quality and filling time were monitored during the experiment, and the results were compared with the simulation predictions of Scheme 3. The key infusion parameters are summarized in Table 3. The total infused resin mass is 365 g, and the actual filling time is 3611 s, while the simulated filling time is 3883 s. The relative error is approximately 7%, which is within an acceptable range. This discrepancy is mainly attributed to the fact that the three-dimensional permeability coefficients of the dry fiber preform were measured at room temperature, whereas the actual wing skin infusion was carried out at an elevated temperature. Elevated temperature reduces resin viscosity, which typically accelerates filling, but also may affect the binder and veil behavior. Therefore, the room temperature permeability data used as input do not fully capture the temperature-dependent flow characteristics. Nevertheless, the 7% error confirms that the simulation based on room temperature permeability is sufficiently reliable for engineering guidance.

Table 3. Resin infusion results of VARI process for wing skin.

Total Infused Resin Mass/g	Filling Time/s	Error Relative to Simulated Filling Time/%
365 g	3611 s	7%

Figure 19 shows the curing and demolding of the wing skin. The infused dry fiber wing skin was placed in an oven and heated according to a preset curing cycle. After completion of the curing process, the component was cooled to room temperature before demolding, followed by the removal of excess resin from its edges and corners. Visual inspection confirmed a defect-free surface on the dry fiber wing skin, which aligned closely with the simulation results. This agreement validates the numerical model as a reliable tool for guiding the resin infusion process in dry fiber composite structures.

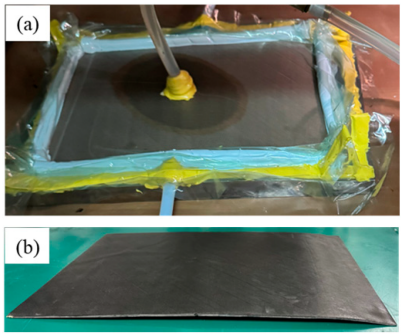

Figure 19. Curing and demolding of composite: (**a**) Resin infusion; (**b**) demolding.

3.3.3. Non-Destructive Testing of the Wing Skin

The non-destructive testing results of the wing skin are shown in Figure 20. Ultrasonic C-scan inspection was performed using a 10 MHz probe, and the evaluation was based on the reflected signal amplitude. The results indicate that the internal structure of the scaled wing skin component is uniform and compact, with no defects such as delamination, inclusions, cracks or interlayer debonding.

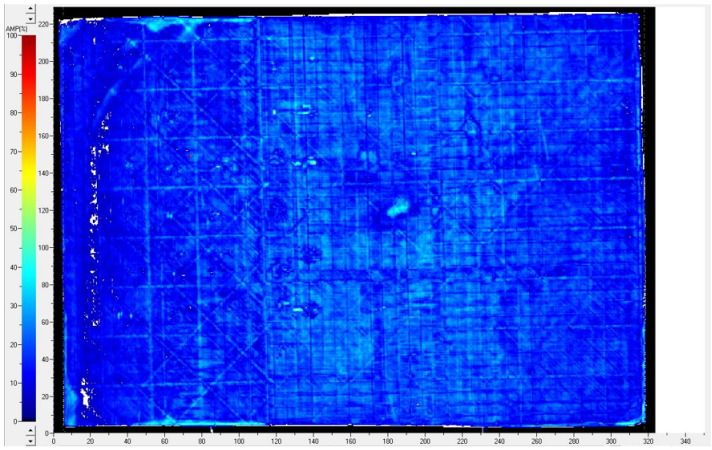

Figure 20. Non-destructive testing results of the wing skin.

4. Conclusions

(1) Using the unsaturated radial flow method combined with ultrasonic measurement method, the three-dimensional permeability of dry fiber preforms produced by automated dry fiber placement (ADFP) was investigated. The results indicate that placement speed is a critical parameter governing interlayer fixation and out-of-plane permeability. An excessively high speed (250 mm/s) leads to partial melting of the veil, resulting in weak interlayer bonding and high permeability, whereas a low speed (150 mm/s) causes complete melting of the veil, providing excellent interlayer fixation but drastically reducing permeability and causing inefficient resin impregnation. A balanced speed of 200 mm/s achieves partial melting of the veil, offering both satisfactory permeability and good interlayer bonding, thus representing the optimal process window for manufacturing wing skin components.

(2) The PAM-RTM software was employed to simulate the infusion process of dry fiber wing skin structures manufactured using the VARI process. Both the simulation and experimental preparation successfully produced high-quality components, with a discrepancy of 7% in the infusion time. This agreement indicates that the numerical model can be reliably applied to analyze and validate the VARI molding process for composite materials. The validated numerical model offers an effective tool for the

pre-design and process optimization of VARI-molded dry fiber composite wing skin components, reducing the cost and cycle of experimental trials.

(3) The discrepancy between the simulation and experimental results mainly arises from the fact that during the actual infusion process of the wing skin preform, the three-dimensional permeability coefficients were measured at room temperature, whereas the real resin infusion was conducted at an elevated temperature, leading to a difference in resin viscosity and flow behavior that causes a slight deviation in the overall infusion time.

(4) Based on the lessons learned from this investigation, several future research directions are suggested. First, the experimental matrix should be extended to include more component geometries (e.g., parts with varying curvatures and thicknesses) and a broader range of placement parameters, so that sufficient data can be collected to enable the future development of empirical or semi-empirical models. Second, systematic studies on the effect of resin temperature and viscosity on infusion behavior using the measured permeability data, possibly incorporating coupled flow–cure simulations, are needed. Third, the proposed framework can be adapted to other liquid molding processes (e.g., RTM) and to other newly emerging dry fiber materials.

Author Contributions: Writing—original draft, Validation, Methodology, Investigation, Formal analysis, Data curation, Conceptualization, W.D. Writing—original draft, Validation, J.L. Writing—original draft, Validation, H.S. Writing—review and editing, Supervision, Resources, Methodology, Conceptualization, M.J. Investigation, B.N., Y.Y. and W.L. Supervision, Resources, K.H. Supervision, Resources, Methodology, Conceptualization, H.Z. Supervision, Resources, Project administration, J.Y. All authors have read and agreed to the published version of the manuscript.

Funding: This research was funded by the Innovation Fund Project of National Commercial Aircraft Manufacturing Engineering Technology Research Center (COMAC-SFGS-2024-717), National Science and Technology Major Project (2024ZD0602200-07), and the Open Project of Shanghai High Performance Fibers and Composites Center (Province-Ministry Joint), Donghua University.

Data Availability Statement: Data available upon request to the authors.

Conflicts of Interest: Authors Bo Ning, Yang Yang and Weiping Liu were employed at Shanghai Aircraft Manufacturing Co., Ltd. The remaining authors declare that the research was conducted in the absence of any commercial or financial relationships that could be construed as a potential conflict of interest.

Abbreviations

The following abbreviations are used in this manuscript:

LCM	Liquid Composite Molding
RTM	Resin Transfer Molding
VARI	Vacuum-Assisted Resin Infusion
AFP	Automated Fiber Placement

References

1. Wang, Y.; Thorn, T.D.S.; Liu, Y.; Advani, S.G.; Papageorgiou, D.G.; Bilotti, E.; Zhang, H. A review on energy-efficient manufacturing for high-performance fibre-reinforced composites. *Compos. Part A Appl. Sci. Manuf.* **2025**, *192*, 108779. [CrossRef]
2. Seong, G.-C.; Kim, D.-K.; Han, W.; Kim, K.-W.; Kim, B.-J. Comparative analysis of carbon fiber reinforced composites: Evaluating recycled carbon fibers as substitutes for commercial grades. *Compos. Part B Eng.* **2025**, *307*, 112932. [CrossRef]
3. Mamat, R.; Rashid, M.I.M.; Syahir, A.Z.; Erdiwansyah, E.; Yusop, A.F.; Tamimi, A. Carbon fibre for applications in aerospace: A review. *J. Alloys Metall. Syst.* **2025**, *12*, 100227. [CrossRef]
4. Liu, Y.-N.; Yuan, C.; Liu, C.; Pan, J.; Dong, Q. Study on the resin infusion process based on automated fiber placement fabricated dry fiber preform. *Sci. Rep.* **2019**, *9*, 7440. [CrossRef]

5. Frketic, J.; Dickens, T.; Ramakrishnan, S. Automated manufacturing and processing of fiber-reinforced polymer (FRP) composites: An additive review of contemporary and modern techniques for advanced materials manufacturing. *Addit. Manuf.* **2017**, *14*, 69–86. [CrossRef]
6. Carosella, S.; Hügle, S.; Helber, F.; Middendorf, P. A short review on recent advances in automated fiber placement and filament winding technologies. *Compos. Part B Eng.* **2024**, *287*, 111843. [CrossRef]
7. Kadiyala, A.K.; Portela, A.; Devlin, K.; Lee, S.; O'Carroll, A.; Jones, D.; Comer, A. Mechanical evaluation and failure analysis of composite laminates manufactured using automated dry fibre tape placement followed by liquid resin infusion. *Compos. Sci. Technol.* **2021**, *201*, 108512. [CrossRef]
8. Bickerton, S.; Govignon, Q.; Kelly, P. Resin infusion/liquid composite moulding (LCM) of advanced fibre-reinforced polymer (FRP). In *Advanced Fibre-Reinforced Polymer (FRP) Composites for Structural Applications*; Woodhead Publishing: Cambridge, UK, 2013; pp. 155–186.
9. Seyednourani, M.; Yildiz, M.; Sas, H.S. A two-stage optimization methodology for gate and vent locations and distribution media layout for liquid composite molding process. *Compos. Part A Appl. Sci. Manuf.* **2021**, *149*, 106522. [CrossRef]
10. Aziz, A.R.; Ali, M.A.; Zeng, X.; Umer, R.; Schubel, P.; Cantwell, W.J. Transverse permeability of dry fiber preforms manufactured by automated fiber placement. *Compos. Sci. Technol.* **2017**, *152*, 57–67. [CrossRef]
11. Di Fratta, C.; Koutsoukis, G.; Klunker, F.; Ermanni, P. Fast method to monitor the flow front and control injection parameters in resin transfer molding using pressure sensors. *J. Compos. Mater.* **2016**, *50*, 2941–2957. [CrossRef]
12. Lee, H.; Jung, K.; Park, H. Study on structural design and analysis of composite boat hull manufactured by resin infusion simulation. *Materials* **2021**, *14*, 5918. [CrossRef]
13. Sarojini Narayana, S.; Khoun, L.; Trudeau, P.; Milliken, N.; Hubert, P. Numerical and experimental investigation of resin flow, heat transfer and cure in a 3D compression resin transfer moulding process using fast curing resin. *Adv. Manuf. Polym. Compos. Sci.* **2024**, *10*, 2378586. [CrossRef]
14. Chai, B.X.; Eisenbart, B.; Nikzad, M.; Fox, B.; Blythe, A.; Blanchard, P.; Dahl, J. Simulation-based optimisation for injection configuration design of liquid composite moulding processes: A review. *Compos. Part A Appl. Sci. Manuf.* **2021**, *149*, 106540. [CrossRef]
15. Lisegaard, J.; Kergomard, Y.D.; Adhikari, D.; Hattel, J.; Mohanty, S. Resin flow models for reinforcement learning for optimal control of LCM. *IOP Conf. Ser. Mater. Sci. Eng.* **2025**, *1338*, 012042.
16. Siddig, N.; Denis, Y.; De Fontgalland, A.; Lecointe, D.; Le Bot, P. Optimization of the infusion process with acrylic resin through physics-based simulation. In *Materials Research Proceedings*; Materials Research Forum LLC: Millersville, PA, USA, 2025; p. 54.
17. Trochu, F.; Ruiz, E.; Achim, V.; Soukane, S. Advanced numerical simulation of liquid composite molding for process analysis and optimization. *Compos. Part A Appl. Sci. Manuf.* **2006**, *37*, 890–902.
18. Laurenzi, S.; Grilli, A.; Pinna, M.; De Nicola, F.; Cattaneo, G.; Marchetti, M. Process simulation for a large composite aeronautic beam by resin transfer molding. *Compos. Part B Eng.* **2014**, *57*, 47–55.
19. Rodrigues, I.; Amico, S.C.; Souza, J.A.; de Lima, A.G.B. Numerical analysis of the resin transfer molding process via PAM-RTM software. *Defect Diffus. Forum* **2015**, *365*, 88–93. [CrossRef]
20. Kozioł, M. Simplified simulation of VARI process using PAM-RTM software. *Compos. Theory Pract.* **2015**, *15*, 218–227.
21. Grössing, H.; Stadlmajer, N.; Fauster, E.; Fleischmann, M.; Schledjewski, R. Flow front advancement during composite processing: Predictions from numerical filling simulation tools in comparison with real-world experiments. *Polym. Compos.* **2016**, *37*, 2782–2793. [CrossRef]
22. Khalili, P.; Kádár, R.; Skrifvars, M.; Blinzler, B. Impregnation behaviour of regenerated cellulose fabric Elium® composite: Experiment, simulation and analytical solution. *J. Mater. Res. Technol.* **2021**, *10*, 66–73. [CrossRef]
23. Magagnato, D.; Seuffert, J.; Bernath, A.; Kärger, L.; Henning, F. Experimental and numerical study of the influence of integrated load transmission elements on filling behavior in resin transfer molding. *Compos. Struct.* **2018**, *198*, 135–143. [CrossRef]
24. Kim, J.-I.; Hwang, Y.-T.; Choi, K.-H.; Kim, H.-J.; Kim, H.-S. Prediction of the vacuum assisted resin transfer molding (VARTM) process considering the directional permeability of sheared woven fabric. *Compos. Struct.* **2019**, *211*, 236–243. [CrossRef]
25. Falaschetti, M.P.; Rondina, F.; Zavatta, N.; Gragnani, L.; Gironi, M.; Troiani, E.; Donati, L. Material characterization for reliable resin transfer molding process simulation. *Appl. Sci.* **2020**, *10*, 1814. [CrossRef]
26. Siddig, N.; Mulye, P.; Le Guennec, Y.; Le Bot, P.; Lecointe, D.; Denis, Y.; Syerko, E.; Fouché, O.; Binetruy, C. Towards the optimization of the infusion process through numerical permeability analysis and simulation. In *Proceedings of the 21st European Conference on Composite Materials (ECCM-21)*; European Society for Composite Materials (ESCM): Nantes, France, 2024; Volume 5.
27. Chen, T.; Wang, T.; Liu, Y.; Guo, M.; Zhou, J.; Zhao, Z.; Yan, B.; Yang, P.; Chen, Z. Numerical simulation study on VARTM processing of large-tow carbon fiber reinforced composite automotive floor panel. In *Proceedings of the 13th Annual International Conference on Material Science and Environmental Engineering (MSEE 2025)*; SPIE (Society of Photo-Optical Instrumentation Engineers): Bellingham, WA, USA, 2025; Volume 13811.

28. Fauster, E.; Berg, D.C.; Abliz, D.; Grössing, H.; Meiners, D.; Ziegmann, G.; Schledjewski, R. Image processing and data evaluation algorithms for reproducible optical in-plane permeability characterization by radial flow experiments. *J. Compos. Mater.* **2019**, *53*, 45–63.
29. Weitzenböck, J.R.; Shenoi, R.A.; Wilson, P.A. Radial flow permeability measurement. Part A: Theory. *Compos. Part A Appl. Sci. Manuf.* **1999**, *30*, 781–796.
30. Ahn, S.H.; Lee, W.I.; Springer, G.S. Measurement of the three-dimensional permeability of fiber preforms using embedded fiber optic sensors. *J. Compos. Mater.* **1995**, *29*, 714–733. [CrossRef]